

Synthesized-Isotropic Narrowband Channel Parameter Extraction from Angle-Resolved Wideband Channel Measurements

Minseok Kim, *Senior Member, IEEE*, Masato Yomoda

Abstract—Angle-resolved channel sounding using antenna arrays or mechanically steered high-gain antennas is widely employed at millimeter-wave and terahertz bands. To extract antenna-independent large-scale channel parameters such as path loss, delay spread, and angular spread, the radiation-pattern effects embedded in the measured responses must be properly compensated. This paper revisits the technical challenges of path-gain calculation from angle-resolved wideband measurements, with emphasis on angular-domain power integration where the scan beams are inherently non-orthogonal and simple power summation leads to biased omni-equivalent power estimates. We first formulate the synthesized-isotropic narrowband power in a unified matrix form and introduce a beam-accumulation correction factor, including an offset-averaged variant to mitigate scalloping due to off-grid angles. The proposed framework is validated through simulations using channel models and 154 GHz corridor measurements.

Index Terms—Channel measurement, angle-scanning, horn antennas, double-directional channel sounding, millimeter-wave channel, terahertz propagation, synthesized-isotropic, path loss, antenna de-embedding.

I. INTRODUCTION

Path loss, defined as the reciprocal of path gain, is a fundamental large-scale parameter for radio system development [1], [2]. In principle, obtaining an antenna-independent path loss determined solely by the propagation channel requires an isotropic antenna assumption [3], [4]. In practice, however, channel measurements at millimeter-wave and terahertz bands typically rely on angle scanning with high-gain antennas or antenna arrays to ensure sufficient link budget and to resolve the angular structure of multipath propagation. Accordingly, double-directional (D-D) channel sounding employs mechanical steering or array-based beamforming at both the transmitter (Tx) and receiver (Rx) [5]–[8]. A challenging task in such measurements is to derive isotropic-equivalent channel parameters (e.g., omni-equivalent path gain/path loss and dispersion metrics) from angle-resolved wideband data.

Conceptually, omni-equivalent power recovery amounts to integrating the measured power over delay and angle. In the delay domain, this is typically well behaved after standard back-to-back calibration [9], [10], so power integration across

M. Kim and M. Yomoda are with the Graduate School of Science and Technology, Niigata University, Niigata 950-2181, Japan (e-mail: mskim@eng.niigata-u.ac.jp).

This work was partly supported by the Commissioned Research through the National Institute of Information and Communications Technology (NICT) (#JPJ012368C02701), and the Ministry of Internal Affairs and Communications (MIC)/FORWARD (#JPMI240410003), Japan.

delay bins provides a consistent estimate of the wideband received power. In contrast, angular-domain integration is fundamentally biased by the non-orthogonality and overlap of practical scan beams depending on angular scanning or sampling interval (ASI). Unlike the delay domain, the spatial beams produced by arrays or horn antennas are inherently non-orthogonal. This leads to a critical trade-off: with a coarse ASI (undersampling), the measurement suffers from scalloping loss, i.e., attenuation of energy arriving between beam centers, which underestimates the omni-equivalent power; with a fine ASI (oversampling) intended to avoid such gaps, adjacent pointings exhibit substantial pattern overlap, and naive power summation over all scanned angles counts correlated contributions from the same propagation path multiple times, resulting in biased overestimation of the omni-equivalent power.

To address these issues, parametric high-resolution estimators such as Space-Alternating Generalized Expectation-maximization (SAGE) [11], Richter's Maximum Likelihood (RIMAX) [12], and CLEAN algorithm [13], [14] incorporate antenna responses to estimate multipath parameters, including Angle of Arrival (AoA), Angle of Departure (AoD), delay, and complex weights, from which an antenna-independent path gain can be obtained by summing the estimated path powers. In practice, however, only a limited set of dominant specular components is typically recovered, and the residual power due to diffuse or unresolvable dense multipath components (DMC) may be missed [15], leading to an underestimation of the total received power and motivating supplementary omnidirectional measurements for PL characterization [6]. By contrast, non-parametric approaches (e.g., beamforming-based angular power spectra) are computationally robust but remain biased due to non-orthogonal beams and sidelobe-induced angular leakage, which distorts angular integration and the resulting omni-equivalent power.

Several studies have addressed omni-/isotropic-equivalent power and path loss (PL) estimation from directional measurements. A practical synthesis of omnidirectional received power and PL from directional scanning measurements has been proposed by combining measurements over multiple pointing angles [16]. The fundamental difficulty of estimating omnidirectional PL from directional sounding, where the same propagation paths may appear in multiple pointings and thus complicate direct power aggregation, has also been discussed [17]. A linear combining framework that accounts for antenna gain patterns and nonuniform angular sampling has been studied for isotropic PL estimation [18]. High-resolution multipath

angle estimation has been developed to improve parameter extraction from power–angle–delay profiles without increasing measurement complexity [19]. In addition, the virtual antenna array (VAA) approach has been investigated for omnidirectional PL measurement using directional antennas [20].

While these methods address important aspects of directional-to-omni recovery, a practical gap remains in obtaining an accurate omni-equivalent received power directly from discretely sampled, non-orthogonal angular beams under realistic scan resolutions. In particular, beam overlap and sidelobe leakage bias angular power integration, and the resulting omni-equivalent metric further depends on the within-bin offset between the true angle and the scan grid (scalloping), which becomes increasingly pronounced for wider beams and/or coarser scan steps. Moreover, a unified framework that is straightforward to implement in various practical measurement configurations is still desirable.

This paper addresses the above gap by presenting an implementation-friendly framework to extract synthesized-isotropic narrowband received power (and the resulting path gain/path loss) from discretely sampled angle-resolved wideband measurements. Specifically, we (i) formulate omni-equivalent power synthesis in a unified matrix form that makes the non-orthogonality and overlap of practical scan beams explicit, and (ii) introduce a beam-accumulation correction factor computed as a discrete summation of the squared antenna pattern over the scan grid, together with an offset-averaged variant that mitigates scalloping without estimating off-grid angles. The proposed framework is validated through channel simulations and 154 GHz corridor measurements.

The remainder of this paper is organized as follows. Sec. II introduces the omnidirectional narrowband and angle-resolved wideband measurement models and the discrete scan-grid representation used throughout. Sec. III presents the synthesized-isotropic power extraction method and the proposed beam-accumulation correction, including an offset-averaged variant to mitigate scalloping. Sec. IV describes how the accumulation factor is computed using an analytic Gaussian beam model and measured horn patterns. Sec. V provides simulation and measurement results, and Sec. VI concludes the paper.

II. MEASUREMENT METHODS

A. Omnidirectional Narrowband Channels

We first consider channel measurements using omnidirectional antennas with narrowband signaling as the traditional approach, in which neither angular nor delay resolution is available as shown in Fig. 1(a). As a result, the received signal represents a superposition of all multipath components (MPCs), leading to small-scale fading due to constructive and destructive interference.

Assuming isotropic antennas at both the Tx and Rx, the narrowband channel response evaluated at the carrier frequency f_c is modeled as a superposition of plane-wave MPCs as

$$H_0 \triangleq \sum_l \gamma_l e^{-j2\pi f_c \tau_l}, \quad (1)$$

where γ_l and τ_l denote the complex amplitude and propagation delay of the l -th MPC, respectively.

The path gain is obtained by taking the ensemble average of the squared magnitude of the complex channel response. Expanding (1) introduces both the power contributions of individual MPCs and cross-terms arising from interference between different paths. Under the widely accepted uncorrelated scattering (US) assumption [21], the phases of different MPCs are statistically uncorrelated. Consequently, the cross-terms vanish after ensemble averaging, and the total average received power can be approximated as

$$P_c = \mathbb{E}\{H_0 \cdot H_0^*\} \approx \sum_l |\gamma_l|^2, \quad (2)$$

where $\mathbb{E}\{\cdot\}$ denotes the ensemble average. This result indicates that, in a rich multipath environment with uncorrelated scatterers, the total received power is given by the incoherent sum of the powers contributed by individual MPCs.

B. Angle-Resolved Wideband Channels

We now extend the above narrowband omnidirectional model to the angle-resolved wideband channel measurement framework. Let us consider an angle-scanning measurement sampled in the angular and frequency domains with a given ASI, as illustrated in Fig. 1(b), and a given frequency resolution within a measurement bandwidth W . The frequency-domain sounding signal is assumed to be known and perfectly equalized. Hence, the influence of the transmitted waveform is removed, and the measured data represent the channel transfer function (CTF).

The measured time-invariant angle-resolved multi-dimensional channel transfer function (MDCTF) [13], [14] is expressed as

$$\begin{aligned} \tilde{H}(\check{f}, \check{\theta}_T, \check{\phi}_T, \check{\theta}_R, \check{\phi}_R) = & \iiint a_R(\check{\theta}_R - \vartheta_R, \check{\phi}_R - \varphi_R) \\ & \cdot H_c(\check{f}, \vartheta_T, \varphi_T, \vartheta_R, \varphi_R) a_T(\check{\theta}_T - \vartheta_T, \check{\phi}_T - \varphi_T) \\ & \cdot \sin \vartheta_T d\vartheta_T d\varphi_T \sin \vartheta_R d\vartheta_R d\varphi_R \\ & + \frac{1}{\sqrt{G_T G_R}} Z(\check{f}, \check{\theta}_T, \check{\phi}_T, \check{\theta}_R, \check{\phi}_R), \end{aligned} \quad (3)$$

where $a_T(\cdot)$ and $a_R(\cdot)$ denote the gain-normalized far-field radiation patterns of the Tx and Rx antennas, respectively, expressed as functions of the angular offset between the antenna pointing direction and the angle of departure or arrival. Here, G_T and G_R denote the peak (boresight) power gains of the Tx and Rx antennas, respectively, and $Z(\cdot)$ represents the additive measurement noise, modeled as zero-mean circularly symmetric complex Gaussian noise. The discrete co-elevation (θ) and azimuth (ϕ) pointing angles at the Tx and Rx are defined as

$$\check{\theta}_T \in \left\{ \theta_{T,n_{\theta_T}} = n_{\theta_T} \Delta_{\theta_T} \mid n_{\theta_T} = 0, \dots, N_{\theta_T} - 1 \right\}, \quad (4)$$

$$\check{\phi}_T \in \left\{ \phi_{T,n_{\phi_T}} = n_{\phi_T} \Delta_{\phi_T} \mid n_{\phi_T} = 0, \dots, N_{\phi_T} - 1 \right\}, \quad (5)$$

$$\check{\theta}_R \in \left\{ \theta_{R,n_{\theta_R}} = n_{\theta_R} \Delta_{\theta_R} \mid n_{\theta_R} = 0, \dots, N_{\theta_R} - 1 \right\}, \quad (6)$$

$$\check{\phi}_R \in \left\{ \phi_{R,n_{\phi_R}} = n_{\phi_R} \Delta_{\phi_R} \mid n_{\phi_R} = 0, \dots, N_{\phi_R} - 1 \right\}. \quad (7)$$

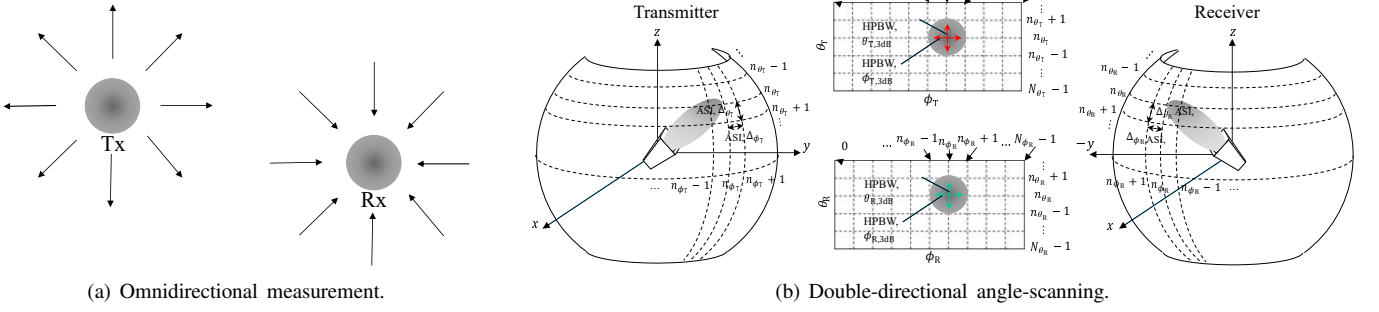


Fig. 1. Omnidirectional measurement vs angle-scanning measurement.

The delay and frequency bins are given by

$$\check{f} \in \{f_{n_f} = f_c + n_f \Delta_f \mid n_f = -N/2, \dots, N/2 - 1\}, \quad (8)$$

$$\check{\tau} \in \{\tau_{n_\tau} = n_\tau \Delta_\tau \mid n_\tau = 0, \dots, N - 1\}, \quad (9)$$

where f_c denotes the center frequency, and n , N , and Δ denote the sample index, the total number of samples, and the ASI in the corresponding domain, respectively. The delay resolution satisfies $\Delta_\tau = 1/(N\Delta_f)$. The propagation channel transfer function

$$H_c(f, \theta_T, \phi_T, \theta_R, \phi_R) = \sum_{l=1}^L \gamma_l e^{-j2\pi f \tau_l} \cdot \frac{1}{\sin \theta_T} \delta(\theta_T - \theta_{T,l}) \delta(\phi_T - \phi_{T,l}) \cdot \frac{1}{\sin \theta_R} \delta(\theta_R - \theta_{R,l}) \delta(\phi_R - \phi_{R,l}), \quad (10)$$

which is expressed by extending (1) to the angular domains. Neglecting the noise term in (3) (high-SNR assumption) and substituting (10) into (3), the MDCTF is obtained as

$$\tilde{H}(\check{f}, \check{\theta}_T, \check{\phi}_T, \check{\theta}_R, \check{\phi}_R) \approx \sum_{l=1}^L \gamma_l a_R(\check{\theta}_R - \theta_{R,l}, \check{\phi}_R - \phi_{R,l}) \cdot a_T(\check{\theta}_T - \theta_{T,l}, \check{\phi}_T - \phi_{T,l}) e^{-j2\pi \check{f} \tau_l}. \quad (11)$$

By applying the inverse Fourier transform to (11), the discrete time-invariant multi-dimensional channel impulse response (MDCIR) sample at multi-dimensional index $\mathbf{n} = [n_\tau, n_{\theta_T}, n_{\phi_T}, n_{\theta_R}, n_{\phi_R}]$ is obtained as

$$\tilde{h}_{\mathbf{n}} = \sum_{l=1}^L \gamma_l A_{\mathbf{n}}(\Omega_l), \quad (12)$$

where $\Omega_l = [\tau_l, \theta_{T,l}, \phi_{T,l}, \theta_{R,l}, \phi_{R,l}]^T$, and the response function for the l -th MPC is defined as

$$A_{\mathbf{n}}(\Omega_l) \triangleq a_u(\tau_{n_\tau} - \tau_l) \cdot a_R(\theta_{R,n_{\theta_R}} - \theta_{R,l}, \phi_{R,n_{\phi_R}} - \phi_{R,l}) \cdot a_T(\theta_{T,n_{\theta_T}} - \theta_{T,l}, \phi_{T,n_{\phi_T}} - \phi_{T,l}). \quad (13)$$

Note that due to the finite measurement bandwidth, the ideal Dirac delta function in the delay domain is replaced by the autocorrelation function of the sounding signal, denoted by $a_u(\tau)$.

By stacking all delay and angular samples into a single column vector $\tilde{\mathbf{h}} \in \mathbb{C}^{N_{\text{tot}} \times 1}$ ($N_{\text{tot}} \triangleq N N_{\theta_T} N_{\phi_T} N_{\theta_R} N_{\phi_R}$), the discrete channel model can be equivalently expressed in vector-matrix form as

$$\tilde{\mathbf{h}} = \sum_{l=1}^L \gamma_l \mathbf{A}(\Omega_l) = \mathbf{A} \boldsymbol{\gamma}, \quad (14)$$

where $\boldsymbol{\gamma} = [\gamma_1, \dots, \gamma_L]^T$, and the matrix $\mathbf{A} = [\mathbf{A}(\Omega_1), \dots, \mathbf{A}(\Omega_L)] \in \mathbb{C}^{N_{\text{tot}} \times L}$ contains the steering vectors for all paths. The steering vector for the l -th path is defined using the Kronecker product as

$$\mathbf{A}(\Omega_l) \triangleq \mathbf{a}_u(\tau_l) \otimes \mathbf{a}_T(\theta_{T,l}, \phi_{T,l}) \otimes \mathbf{a}_R(\theta_{R,l}, \phi_{R,l}). \quad (15)$$

The constituent vectors are defined as

$$\begin{aligned} [\mathbf{a}_u(\tau_l)]_{n_\tau} &\triangleq a_u(\tau_{n_\tau} - \tau_l) \\ [\mathbf{a}_T(\theta_{T,l}, \phi_{T,l})]_{n_{\theta_T}, n_{\phi_T}} &\triangleq a_T(\theta_{T,n_{\theta_T}} - \theta_{T,l}, \phi_{T,n_{\phi_T}} - \phi_{T,l}), \\ [\mathbf{a}_R(\theta_{R,l}, \phi_{R,l})]_{n_{\theta_R}, n_{\phi_R}} &\triangleq a_R(\theta_{R,n_{\theta_R}} - \theta_{R,l}, \phi_{R,n_{\phi_R}} - \phi_{R,l}). \end{aligned}$$

III. CHANNEL PARAMETER CALCULATION

A. Path Gain

The multi-dimensional channel power vector is defined as the expected element-wise squared magnitude of the MDCIR vector. Assuming the path phases are random and uncorrelated, the cross-terms in the expansion average to zero [13], namely

$$\begin{aligned} \mathbf{P} &\triangleq \mathbb{E}\left\{\tilde{\mathbf{h}} \odot \tilde{\mathbf{h}}^*\right\} = \mathbb{E}\{(\mathbf{A}\boldsymbol{\gamma}) \odot (\mathbf{A}\boldsymbol{\gamma})^*\} \\ &= \mathbb{E}\left\{\sum_{l=1}^L |\gamma_l|^2 |\mathbf{A}_l|^2 + \sum_{\substack{l, l'=1 \\ l' \neq l}} \gamma_l \gamma_{l'}^* (\mathbf{A}_l \odot \mathbf{A}_{l'}^*)\right\} \\ &\approx \sum_{l=1}^L |\gamma_l|^2 |\mathbf{A}_l|^2, \end{aligned} \quad (16)$$

where \mathbf{A}_l denotes $\mathbf{A}(\Omega_l)$ for simplicity, and \odot denotes the Hadamard (element-wise) product. This can be rewritten in matrix notation as

$$\mathbf{P} = \mathbf{B} \mathbf{p} \in \mathbb{R}^{N_{\text{tot}} \times 1}, \quad (17)$$

where $\mathbf{B} = |\mathbf{A}|^2 = \mathbf{A} \odot \mathbf{A}^* \in \mathbb{R}^{N_{\text{tot}} \times L}$ is the basis matrix of component-wise power responses, and $\mathbf{p} = \boldsymbol{\gamma} \odot \boldsymbol{\gamma}^* \in \mathbb{R}^{L \times 1}$ is the vector of path powers.

For analytical and computational tractability, the continuous MPC parameter space is commonly discretized onto a fixed grid. By assuming that the channel gain within each grid cell is approximately constant and grouping the MPCs associated with each cell, (17) is approximated as

$$\mathbf{P} \approx \mathbf{B}_g \mathbf{p}_g \in \mathbb{R}^{N_{\text{tot}} \times 1}, \quad (18)$$

where $\mathbf{B}_g \in \mathbb{R}^{N_{\text{tot}} \times N_{\text{tot}}}$ represents the dictionary matrix of power responses defined at the grid centers, and $\mathbf{p}_g \in \mathbb{R}^{N_{\text{tot}} \times 1}$ denotes the discrete power distribution across the grid, whose elements are not necessarily obtained explicitly, unlike in MPC parameter extraction [13].

Finally, the true channel power P_c , defined as the sum of the powers of all MPCs, is given by

$$P_c \triangleq \sum_{l=1}^L |\gamma_l|^2 = \sum_{k=1}^{N_{\text{tot}}} [\mathbf{p}_g]_k = \mathbf{1}_{N_{\text{tot}}}^T \mathbf{p}_g, \quad (19)$$

where $\mathbf{1}_v \in \mathbb{R}^{v \times 1}$ denotes the all-ones vector. In principle, \mathbf{p}_g can be obtained from (18) as

$$\mathbf{p}_g \approx \mathbf{B}_g^{-1} \mathbf{P}, \quad (20)$$

but explicitly inverting the large matrix \mathbf{B}_g is computationally expensive and often unstable.

Instead, we exploit the property that the column sums of \mathbf{B}_g are constant. This arises from the rotational invariance of the measurement scan, where the same antenna pattern is swept across the grid. This property is expressed as

$$\mathbf{1}_{N_{\text{tot}}}^T \mathbf{B}_g = \zeta \mathbf{1}_{N_{\text{tot}}}^T, \quad (21)$$

where ζ is the total beam accumulation factor. It is obtained by the sum of the elements of any column m of the basis matrix as

$$\zeta = \sum_{n=1}^{N_{\text{tot}}} [\mathbf{B}_g]_{n,m}. \quad (22)$$

Premultiplying (18) by $\mathbf{1}_{N_{\text{tot}}}^T$ yields

$$\begin{aligned} \mathbf{1}_{N_{\text{tot}}}^T \mathbf{P} &= \mathbf{1}_{N_{\text{tot}}}^T \mathbf{B}_g \mathbf{p}_g \\ &\approx \zeta \mathbf{1}_{N_{\text{tot}}}^T \mathbf{p}_g = \zeta P_c. \end{aligned} \quad (23)$$

Therefore, the channel power (synthesized path gain) can be estimated directly from the measured power as

$$P_c = \mathbf{1}_{N_{\text{tot}}}^T \mathbf{p}_g \approx \frac{1}{\zeta} \mathbf{1}_{N_{\text{tot}}}^T \mathbf{P} = \frac{1}{\zeta} \sum_{k=1}^{N_{\text{tot}}} [\mathbf{P}]_k, \quad (24)$$

where ζ acts as a correction factor accounting for beam-overlap effects.

B. Correction Factors

Since the basis matrix \mathbf{B}_g is constructed from the Kronecker product of the delay and angular responses, the total beam accumulation factor ζ in (22) can be factorized into the product of the contributions from each domain as

$$\zeta = \zeta_\tau \cdot \zeta_T \cdot \zeta_R, \quad (25)$$

where ζ_τ , ζ_T , and ζ_R represent the accumulation factors for the delay, Tx angle, and Rx angle domains, respectively.

The delay-domain factor is determined by the column sum of the delay basis matrix. The elements of the delay dictionary are given by

$$[\mathbf{B}_{g,\tau}]_{n,m} = |a_u(\tau_n - \tau_m)|^2, \quad (26)$$

with $\tau_n = n\Delta_\tau$ and $\tau_m = m\Delta_\tau$ for $n, m \in \{0, \dots, N_\tau - 1\}$. For any column m , the accumulation factor is formally defined as

$$\zeta_\tau = \sum_{n=0}^{N_{\text{tot}}-1} [\mathbf{B}_{g,\tau}]_{n,m}, \quad (27)$$

where $N_{\text{tot}} \triangleq N_\tau$. Since the autocorrelation function $a_u(\tau)$ depends only on the delay difference, this summation is shift-invariant (assuming a periodic grid or negligible edge effects). Therefore, (27) simplifies to the sum of the squared autocorrelation samples

$$\zeta_\tau = \sum_{n=0}^{N_{\text{tot}}-1} |a_u(n\Delta_\tau)|^2. \quad (28)$$

Similarly, the angular-domain factors are determined by the summation of the squared antenna pattern samples. The elements of the angular dictionary for a 2D scan are defined as

$$[\mathbf{B}_{g,a}]_{n,m} = |a(\theta_{n_\theta} - \theta_{m_\theta}, \phi_{n_\phi} - \phi_{m_\phi})|^2, \quad (29)$$

where $\theta_{n_\theta} = n_\theta \Delta_\theta$, $\theta_{m_\theta} = m_\theta \Delta_\theta$, $\phi_{n_\phi} = n_\phi \Delta_\phi$, and $\phi_{m_\phi} = m_\phi \Delta_\phi$ with angular indices $n_\theta, m_\theta \in \{0, \dots, N_\theta - 1\}$ and $n_\phi, m_\phi \in \{0, \dots, N_\phi - 1\}$. The indices $n = n_\phi + n_\theta N_\phi$ and $m = m_\phi + m_\theta N_\phi$ denote the linear indices for the observation and grid points, respectively. The function $a(\cdot)$ represents the 2D antenna radiation pattern.

The angular accumulation factor is then obtained by summing the elements of any column m as

$$\zeta_a = \sum_{n=0}^{N_{\text{tot}}-1} [\mathbf{B}_{g,a}]_{n,m}, \quad (30)$$

where $N_{\text{tot}} \triangleq N_\theta N_\phi$. The angular accumulation factor ζ_a in (30) is simply calculated by summing the squared magnitude of the antenna radiation pattern $a(\cdot)$ over all discrete scan angles

$$\zeta_a = \sum_{n_\theta=0}^{N_\theta-1} \sum_{n_\phi=0}^{N_\phi-1} |a(n_\theta \Delta_\theta, n_\phi \Delta_\phi)|^2. \quad (31)$$

Furthermore, if the 2D antenna pattern can be approximated as separable in the co-elevation (Co-El) and azimuth (Az) domains (i.e., $|a(\theta, \phi)|^2 \approx |a_\theta(\theta)|^2 \cdot |a_\phi(\phi)|^2$), the 2D correction factor can be decomposed into the product of two 1D factors as

$$\zeta_a \approx \left(\sum_{n_\theta=0}^{N_\theta-1} |a_\theta(n_\theta \Delta_\theta)|^2 \right) \cdot \left(\sum_{n_\phi=0}^{N_\phi-1} |a_\phi(n_\phi \Delta_\phi)|^2 \right) \quad (32)$$

$$= \zeta_\theta \cdot \zeta_\phi, \quad (33)$$

where ζ_θ and ζ_ϕ represent the beam accumulation factors for the Co-El and Az scans, respectively.

Based on this formulation, the correction factors for various measurement configurations are derived as follows.

1) *Omnidirectional Wideband Case*: In this case, isotropic antennas are assumed ($\zeta_T = \zeta_R = 1$), and the system provides only delay resolution. The autocorrelation function of the sounding signal is defined as the Dirichlet kernel [14] as

$$a_u(\tau) = \frac{1}{N} e^{-j\pi\Delta_f\tau} \frac{\sin(\pi N\Delta_f\tau)}{\sin(\pi\Delta_f\tau)}. \quad (34)$$

For a standard wideband measurement where the delay grid matches the sampling interval ($\Delta_\tau = 1/W$), the orthogonality of the Dirichlet kernel implies that the delay accumulation factor is unity ($\zeta_\tau = 1$). Consequently, the total correction factor simplifies to

$$\zeta = \zeta_\tau \cdot \zeta_T \cdot \zeta_R = 1 \cdot 1 \cdot 1 = 1. \quad (35)$$

Thus, no correction is required, and the total channel power is obtained simply by summing the samples of the power delay profile.

2) *AoA-Resolved Narrowband Case*: In this case, the system employs angular scanning at the receiver but lacks delay resolution ($\zeta_\tau = 1$). Assuming an isotropic Tx ($\zeta_T = 1$), the total factor is determined solely by the Rx's beam overlap as

$$\zeta = \zeta_R \approx \zeta_{\theta_R} \zeta_{\phi_R}. \quad (36)$$

3) *AoD-Resolved Narrowband Case*: Similarly, if angular scanning is performed only at the Tx with an isotropic Rx ($\zeta_R = 1$), the correction factor becomes

$$\zeta = \zeta_T \approx \zeta_{\theta_T} \zeta_{\phi_T}. \quad (37)$$

4) *Double-Directional Angle-Resolved Case*: If angular scanning is performed both at the Tx and Rx, the correction factor becomes

$$\zeta = \zeta_T \zeta_R \approx \zeta_{\theta_T} \zeta_{\phi_T} \zeta_{\theta_R} \zeta_{\phi_R}. \quad (38)$$

C. Delay Spread

For PL evaluation and comparison with conventional omnidirectional wideband measurements, it is often useful to collapse the angle-resolved multidimensional power vector $\mathbf{P} \in \mathbb{R}^{N_{\text{tot}} \times 1}$ into a delay-only power delay profile (PDP) vector. Let N_τ denote the number of delay bins, and define the number of angular scan points at the Tx and Rx as

$$N_T \triangleq N_{\theta_T} N_{\phi_T}, \quad N_R \triangleq N_{\theta_R} N_{\phi_R}, \quad (39)$$

such that $N_{\text{tot}} = N_\tau N_R N_T$. Using the same stacking order implied by the Kronecker-structured response model in (15), the angle-collapsed (synthesized) PDP vector $\mathbf{P}_\tau \in \mathbb{R}^{N_\tau \times 1}$ is obtained by summing over all Tx/Rx scan angles and compensating for the composite beam-overlap gain in the angular domains:

$$\mathbf{P}_\tau \triangleq \frac{1}{\zeta_T \zeta_R} (\mathbf{I}_{N_\tau} \otimes \mathbf{1}_{N_R}^T \otimes \mathbf{1}_{N_T}^T) \mathbf{P}, \quad (40)$$

where \mathbf{I}_{N_τ} is the $N_\tau \times N_\tau$ identity matrix.

If the antenna is mounted such that its center of rotation coincides with its phase center, the angular scan does not introduce any geometry-induced path-length variation (i.e., phase center eccentricity). In this ideal configuration, steering the antenna only changes the angular weighting of the incoming

MPCs based on the antenna radiation pattern. Consequently, the beam-overlap correction factor (e.g., $1/(\zeta_T \zeta_R)$ for the D-D case) acts as a global scalar multiplier on the synthesized omnidirectional PDP and does not modify its delay-domain shape.

Since the RMS delay spread (DS) is computed from the normalized PDP as

$$\sigma_\tau = \sqrt{\frac{\sum_n \tau_n^2 [\mathbf{P}_\tau]_n}{\sum_n [\mathbf{P}_\tau]_n} - \left(\frac{\sum_n \tau_n [\mathbf{P}_\tau]_n}{\sum_n [\mathbf{P}_\tau]_n} \right)^2}, \quad (41)$$

any constant scaling factor applied to \mathbf{P}_τ cancels out in the numerator and denominator. Therefore, the DS estimate is invariant to the beam-overlap correction. It follows that the correction factor is critical for the accuracy of the absolute path gain but does not impact the delay dispersion characteristics.

IV. BEAM ACCUMULATION FACTOR FOR ANTENNA PATTERNS

A. Analytic Model

In this study, a simplified 2D Gaussian beam pattern is constructed utilizing separable Von Mises functions [22], [23]¹ for the El (θ) and Az (ϕ) components. The total radiation pattern is expressed as:

$$a(\theta, \phi) = a_\theta(\theta) a_\phi(\phi), \quad (42)$$

where the directional components for a given angular dimension $\{\theta, \phi\}$ is modeled respectively as

$$a_\theta(\theta) = e^{\kappa_\theta(\cos \theta - 1)}, \quad a_\phi(\phi) = e^{\kappa_\phi(\cos \phi - 1)}, \quad (43)$$

which denote the normalized Von Mises functions (peak unity), and we use the power gain $G(\kappa_\theta, \kappa_\phi)$ calculated as

$$G(\kappa_\theta, \kappa_\phi) = G_\theta(\kappa_\theta) G_\phi(\kappa_\phi), \quad (44)$$

where

$$G_\theta(\kappa_\theta) = \frac{e^{\kappa_\theta}}{I_0(\kappa_\theta)}, \quad G_\phi(\kappa_\phi) = \frac{e^{\kappa_\phi}}{I_0(\kappa_\phi)}. \quad (45)$$

The concentration parameters κ_θ and κ_ϕ is determined by the half-power beamwidths (HPBWs), $\theta_{3\text{dB}}$ and $\phi_{3\text{dB}}$, as

$$\kappa_\theta = \frac{\ln \sqrt{2}}{1 - \cos(0.5\theta_{3\text{dB}})}, \quad \kappa_\phi = \frac{\ln \sqrt{2}}{1 - \cos(0.5\phi_{3\text{dB}})}, \quad (46)$$

where $I_m(\cdot)$ denotes the modified Bessel function of the first kind of order m . This formulation ensures that the generated pattern satisfies the specified HPBW requirements in the principal planes.

The von-Mises-based Gaussian beam model is adopted not only as a simple main-lobe approximation but also for its analytical tractability [22]. Because the von Mises kernel admits a Fourier-Bessel expansion, key quantities required for power synthesis can be derived in closed or semi-closed forms. This enables fast evaluation and parameter sweeps over HPBW and ASI without resorting to heavy numerical integration. Fig. 2 depicts the Az radiation patterns of the Gaussian beam models $G \cdot a(\theta, \phi)$ at $\theta = 90^\circ$, configured with various

¹A slightly modified von-Mises-based formulation is used to facilitate HPBW tuning (i.e., to match a prescribed HPBW more directly).

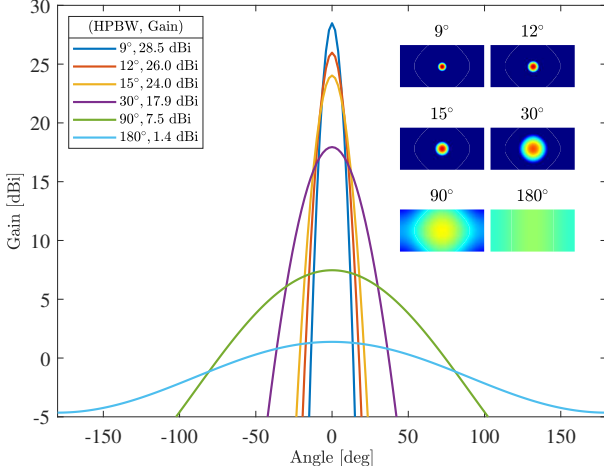


Fig. 2. Radiation patterns of Gaussian beams given by $G \cdot a(\theta, \phi)$ ($\phi_{3\text{dB}} = \theta_{3\text{dB}}$).

HPBWs. In each angular dimension, an omnidirectional (flat) response corresponds to a beamwidth that spans the entire scan domain. Thus, the omni condition is $\phi_{3\text{dB}} = 360^\circ$ for Az ($\phi \in [0, 360^\circ]$) and $\theta_{3\text{dB}} = 180^\circ$ for Co-El ($\theta \in [0, 180^\circ]$). In implementation, we set $\kappa_\theta = 0$ and $\kappa_\phi = 0$ when $\theta_{3\text{dB}}$ and $\phi_{3\text{dB}}$ are equal to or larger than the corresponding domain, yielding $a_\theta(\theta) = 1$ and $a_\phi(\phi) = 1$, respectively.

As established in Sec. III, the synthesized normalization relies on the angular accumulation factor ζ , defined as the sum of the squared antenna pattern samples over the discrete scan grid. By leveraging the separability of the directional antenna model, the 2D angular accumulation factor factorizes into 1D components. In this study, we avoid the continuous-domain approximation and evaluate the accumulation factor directly on the discrete scan grid, since the scan interval Δ_ψ is not necessarily fine compared to the antenna HPBW.

Substituting the antenna model into the definition of the 1D accumulation factor yields the discrete form

$$\zeta_\psi = \sum_{n=0}^{N_\psi-1} \frac{1}{e^{\kappa_\psi} I_0(\kappa_\psi)} e^{2\kappa_\psi \cos(n\Delta_\psi)}, \quad (47)$$

which is computed numerically for the given scan grid $\{n\Delta_\psi\}_{n=0}^{N_\psi-1}$.

For uniform full-Az scanning, i.e., $\Delta_\psi = 360^\circ/N_\psi$, (47) can be rewritten exactly using the Fourier-Bessel expansion of the von Mises kernel as

$$\zeta_\psi = \frac{N_\psi}{e^{\kappa_\psi} I_0(\kappa_\psi)} \left[I_0(2\kappa_\psi) + 2 \sum_{k=1}^{\infty} I_{kN_\psi}(2\kappa_\psi) \right]. \quad (48)$$

In practice, (47) is evaluated directly; alternatively, (48) provides an exact reference expression whose series can be truncated when higher-order terms become negligible.

B. Scalloping Loss Mitigation

The accumulation factor in (30) is constant across grid columns when the MPC angles coincide with the angular grid centers. In practice, the true angles of MPCs are continuous and generally off-grid, which leads to a grid-dependent gain

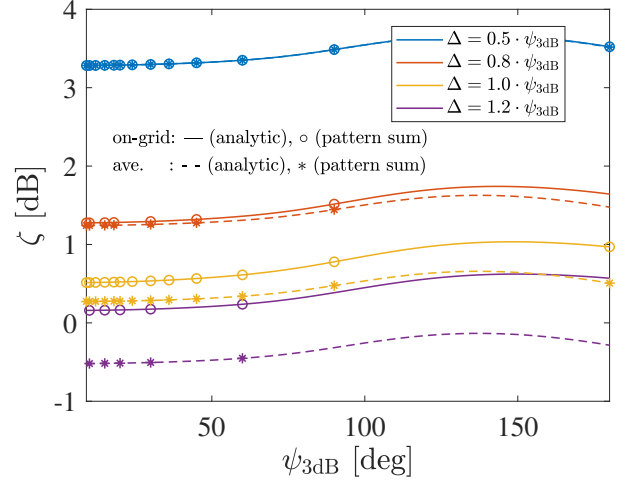


Fig. 3. Variation of the 1D beam-accumulation factor versus HPBW and ASI for Gaussian beam models. The on-grid accumulation factor is computed by the discrete summation in (47) (markers) and by the exact series expression in (48) for uniform full-azimuth scans (solid lines). Furthermore, the within-bin averaged factor is given by (50) (markers) and by the exact series expression in (51) (dashed lines).

variation (scalloping loss) with respect to the within-bin angular offset. To incorporate this effect without explicitly estimating the offset, we use the within-bin average accumulation factor.

For a 1D scan in an angular dimension $\psi \in \{\theta, \phi\}$ with scan interval Δ_ψ and N_ψ scan points, let $\delta_\psi \in [0, \Delta_\psi]$ denote the angular offset from the nearest grid point. The scalloping-loss-aware 1D accumulation factor is defined as

$$\zeta_\psi(\delta_\psi) \triangleq \sum_{n=0}^{N_\psi-1} |a_\psi(n\Delta_\psi - \delta_\psi)|^2. \quad (49)$$

Specifically, for a scan interval Δ_ψ , we average the discrete-grid accumulation over a uniformly distributed offset $\delta \sim \mathcal{U}[0, \Delta_\psi]$ as

$$\bar{\zeta}_\psi \triangleq \frac{1}{\Delta_\psi} \int_0^{\Delta_\psi} \zeta_\psi(\delta) d\delta. \quad (50)$$

In numerical implementation, (50) is obtained by sampling δ densely over $[0, \Delta_\psi]$ and averaging the corresponding $\zeta_\psi(\delta)$ values.

Using the von-Mises Gaussian beam in (42), we can rewrite (48) as

$$\zeta_\psi(\delta) = \frac{N_\psi}{e^{\kappa_\psi} I_0(\kappa_\psi)} \left[I_0(2\kappa_\psi) + 2 \sum_{m=1}^{\infty} I_{mN_\psi}(2\kappa_\psi) \cos(mN_\psi \delta) \right]. \quad (51)$$

Taking the within-bin average over $\delta \in [0, \Delta_\psi]$ removes all cosine terms, yielding the closed-form expression as

$$\bar{\zeta}_\psi = \frac{N_\psi}{e^{\kappa_\psi} I_0(\kappa_\psi)} I_0(2\kappa_\psi). \quad (52)$$

Fig. 3 shows the 1D beam-accumulation factor as a function of HPBW and ASI. The solid curves are computed from the exact series in (48) (uniform full-azimuth scan), while the markers are obtained by the direct discrete summation

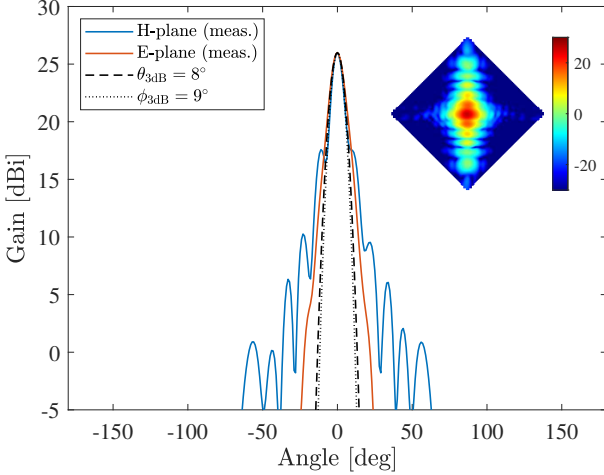


Fig. 4. Radiation patterns of pyramidal horn antenna ($G = 26$ dBi, $\theta_{3dB} \approx 8^\circ$, $\phi_{3dB} \approx 9^\circ$) [23].

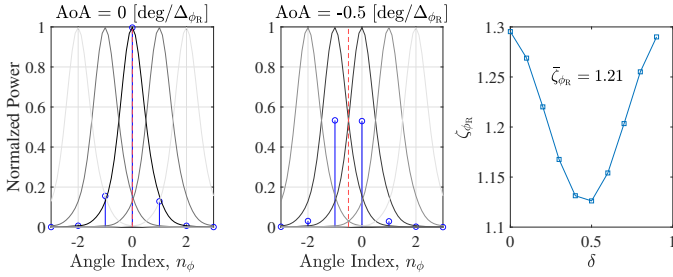


Fig. 5. Illustration of scalloping loss and offset-dependent beam accumulation: normalized received power versus angular index for the on-grid and half-bin-offset AoA cases, and the resulting accumulation factor $\zeta_{\phi_R}(\delta)$ as a function of the within-bin angular offset δ ; the averaged value is $\bar{\zeta}_{\phi_R} = 1.21$.

in (47). The markers are plotted only when the number of scan samples is an integer, i.e., $\Delta_\phi = 360^\circ/N_\phi$ with integer N_ϕ , to ensure the uniform periodic grid assumed in (48). The results confirm that ζ_ψ is mainly governed by the sampling density relative to the beamwidth: smaller Δ_ψ/ψ_{3dB} increases ζ_ψ due to stronger beam overlap. This trend highlights that ζ_ψ is primarily governed by the relative sampling density with respect to the beamwidth, rather than the beamwidth alone. Fig. 3 also presents the within-bin averaged factor $\bar{\zeta}_\psi$ in (50) as a scalloping-robust correction.

C. Measured Antenna Patterns

To evaluate the beam accumulation factor, we employ measured radiation patterns of a pyramidal horn antenna (WR6.5, 154 GHz) [23], [24] obtained from a 2D angular scan. Fig. 4 compares the measured H-plane and E-plane cuts with the Gaussian beam profiles using the same HPBWs. The measured and modeled patterns agree well in the main-lobe region, while the measured E-plane exhibits noticeable sidelobes that are not captured by the Gaussian model.

Fig. 5 provides an intuitive Az scanning example of scalloping in practical directional scans using the measured horn pattern in linear scale. The normalized received power (left) is shown for two AoA cases: an on-grid arrival and a half-bin offset arrival, which yields a lower peak response due to

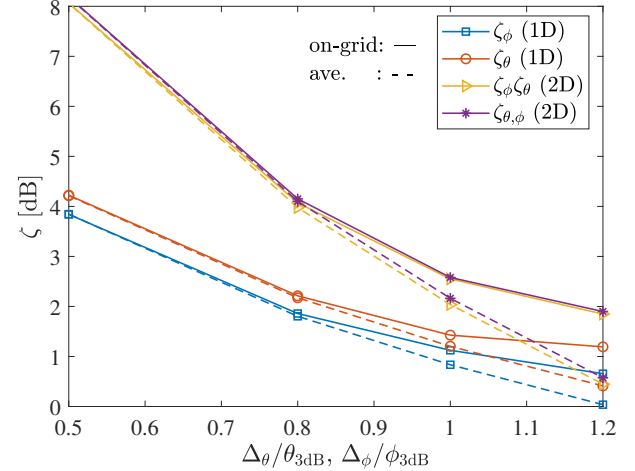


Fig. 6. Beam-accumulation factor of the horn antenna as a function of the ASI.

TABLE I
CORRECTION FACTORS (ζ_{tot}) FOR VARIOUS CONFIGURATIONS USING THE HORN ANTENNAS SHOWN IN FIG. 4.

| Scan domain | | Correction factor | | |
|-------------|-----------|---|--------------|-----------|
| Tx | Rx | ζ_{tot} | On-grid [dB] | Ave. [dB] |
| Az-omni | Az | ζ_{ϕ_R} | 1.12 | 0.83 |
| El-omni | Co-El | ζ_{θ_R} | 1.43 | 1.21 |
| Isotropic | Az, Co-El | $\zeta_{\phi_R} \zeta_{\theta_R}$ | 2.55 | 2.04 |
| Az | Az | $\zeta_{\phi_R} \zeta_{\phi_R}$ | 2.25 | 1.67 |
| Az, El | Az, Co-El | $\zeta_{\phi_T} \zeta_{\theta_T} \zeta_{\phi_R} \zeta_{\theta_R}$ | 5.10 | 4.08 |

the within-bin angular mismatch. The corresponding within-bin accumulation factor $\zeta_{\phi_R}(\delta)$ (right) varies with the offset $\delta \in [0, \Delta_\phi]$, and its average over δ gives $\bar{\zeta}_{\phi_R} = 1.21$, which is used as the offset-averaged correction in the subsequent PL synthesis.

Fig. 6 further shows the beam accumulation factor computed directly from the measured horn patterns as a function of the ASI, expressed in a normalized form relative to the measured HPBW. Consistent with the analytic observation in Fig. 3, the accumulation factor decreases as the scan becomes coarser, because the beam overlap between adjacent pointing directions diminishes. This result provides a practical lookup for selecting the appropriate correction factor under a given scan grid when measured antenna patterns are available.

Table I lists the total beam-accumulation correction factors ζ_{tot} for representative scan configurations using the measured horn patterns in Fig. 4. Here, ζ_{tot} is given by the product of the relevant 1D/2D accumulation factors in the scanned domains (e.g., AZ/Co-El at Tx/Rx), while the last two columns report ζ_{tot} in dB for the on-grid and within-bin averaged corrections, respectively.

V. EVALUATIONS

Although the correction factor has been formulated, the estimation accuracy of the synthesized power can vary depending on the multipath channel conditions. Therefore, we validate the effectiveness of the proposed correction factor through numerical simulations.

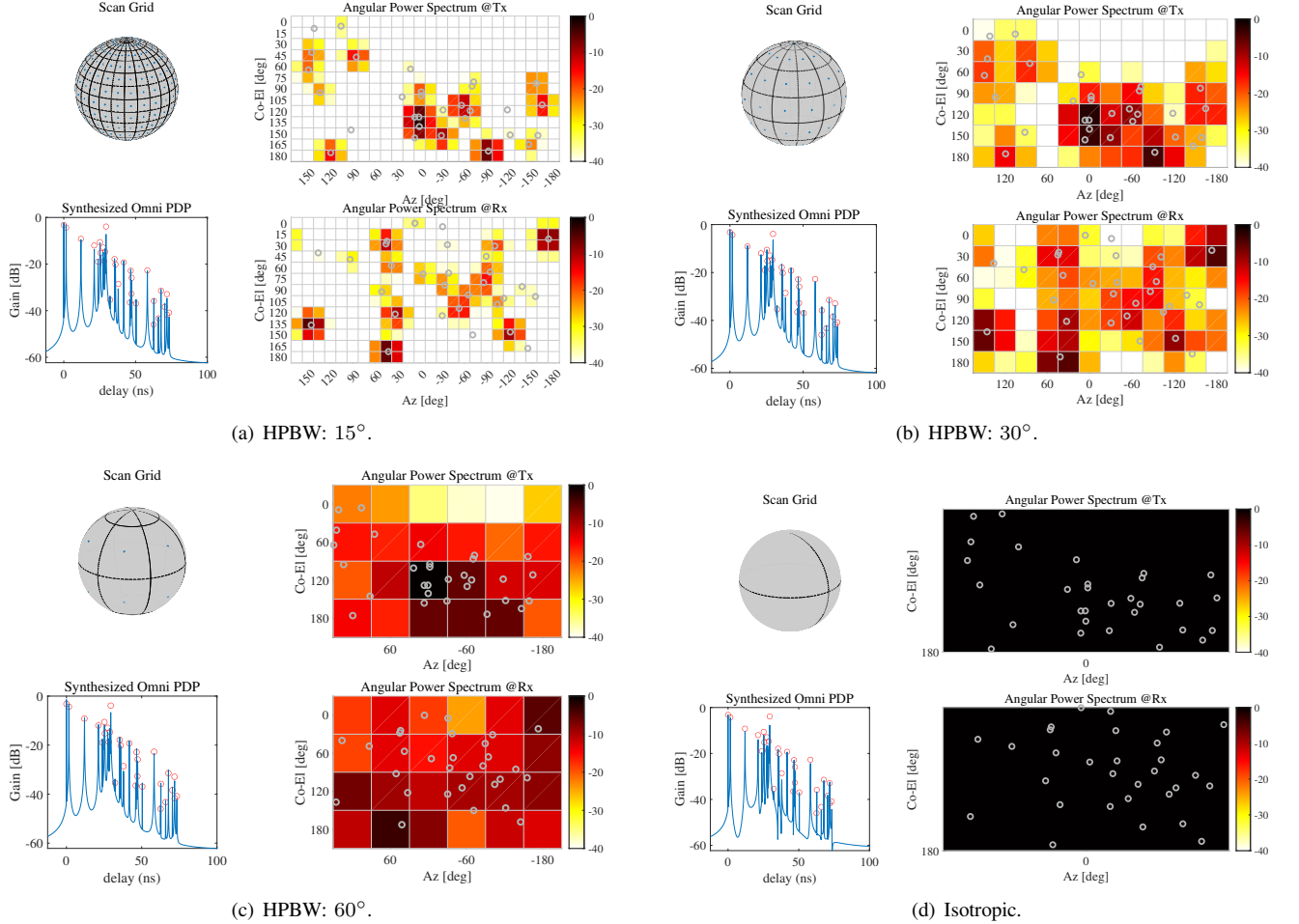


Fig. 7. Synthesized power spectra as a function of the antenna HPBW, assuming identical HPBWs in Co-El and Az at both Tx and Rx ($\theta_{T,3dB} = \phi_{T,3dB} = \theta_{R,3dB} = \phi_{R,3dB}$). The markers indicate the MPCs in delay and AoD/AoA angle domains.

A. Simulation Using A Channel Model

1) *Channel Model*: The underlying propagation channel is generated using a classical Saleh–Valenzuela (SV)-type clustered multipath model [25]. Cluster arrivals follow a Poisson process with rate Λ , and intra-cluster ray arrivals follow a Poisson process with rate λ . Let T_k denote the arrival time of the k -th cluster, and $\tau_{k,l}$ denote the absolute delay of the l -th ray within the k -th cluster. The average power of the l -th ray in the k -th cluster decays exponentially in both the cluster and ray levels as

$$\mathbb{E}\{P_{k,l}\} = \Xi_k \exp\left(-\frac{T_k}{\varrho}\right) \exp\left(-\frac{\tau_{k,l} - T_k}{\rho}\right), \quad (53)$$

where ϱ and ρ are the cluster- and ray-level decay constants, respectively, and Ξ_k models cluster-to-cluster shadowing by a lognormal factor. Each ray is assigned a complex gain

$$\gamma_{k,l} = \sqrt{P_{k,l}} \nu_{k,l}, \quad \nu_{k,l} \sim \mathcal{CN}(0, 1), \quad (54)$$

and an additional independent random phase can be applied in each Monte-Carlo trial to enforce uncorrelated scattering across MPCs.

For the angular domain, each cluster is assigned a mean departure/arrival direction. The cluster mean Az angles are

drawn uniformly over $[0, 2\pi]$, while the cluster mean zenith (co-elevation) angles are concentrated around broadside (near $\theta \approx 90^\circ$). Individual ray angles are generated by adding independent Laplacian-distributed offsets to the corresponding cluster mean angles as

$$\phi = \bar{\phi}_k + \Delta\phi, \quad \text{and} \quad \theta = \bar{\theta}_k + \Delta\theta, \quad (55)$$

where $\Delta\phi$ and $\Delta\theta$ follow Laplacian distributions whose spreads are controlled by the prescribed Az/Co-El angular-spread (AS) parameters.

2) *Simulation Parameters*: We set the channel model parameters as $\varrho = 10$ ns and $\rho = 5$ ns, which implies $\Lambda = 1/\varrho$ and $\lambda = 1/\rho$. Hence, the mean inter-arrival times are $1/\Lambda = \varrho$ for clusters and $1/\lambda = \rho$ for rays, controlling the delay-domain sparsity and the number of effective MPCs. To stress-test the proposed power synthesis and the beam-accumulation correction under a highly diffuse condition, we also consider a wide-spread case with $(\sigma_\phi, \sigma_\theta) = (100^\circ, 100^\circ)$. This wide-spread configuration increases the probability that MPCs populate the full angular domain and is effective for evaluating residual grid-dependence (e.g., HPBW-dependent bias), particularly in Co-El scanning. The cluster-to-cluster large-scale variability is modeled by a lognormal shadowing term with standard

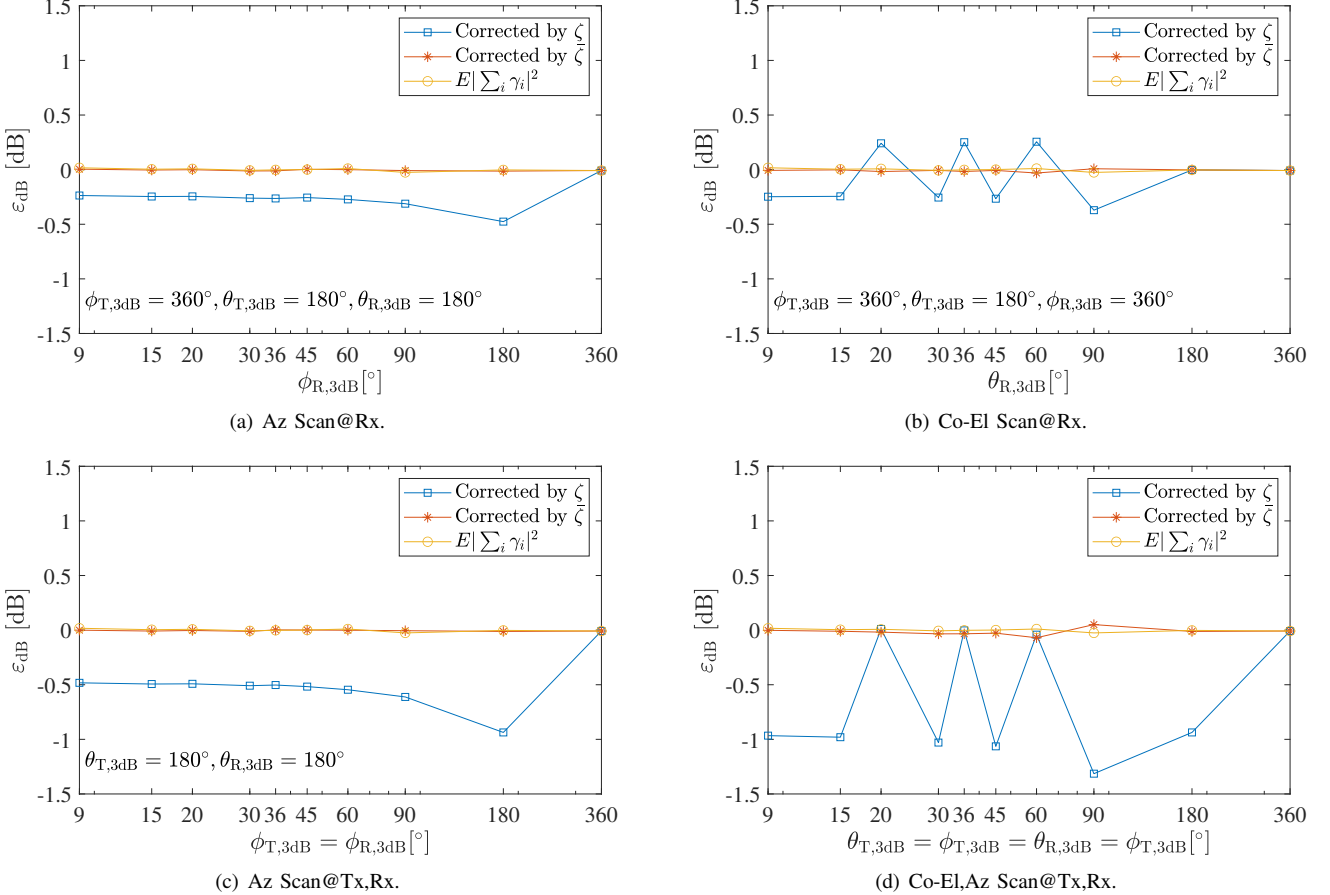


Fig. 8. Path gain estimation error versus HPBW for various directional scanning configurations, evaluated relative to the incoherent power sum $P_c = \sum |\gamma_i|^2$.

deviation $\sigma_{cl} = 3$ dB applied to the cluster power level. This term emulates random fluctuations of dominant clusters across realizations and avoids unrealistically deterministic cluster amplitudes. Assuming sub-terahertz communications, we set the bandwidth to 4 GHz (delay bin resolution is 250 ps).

3) *Evaluation Results:* For a given antenna HPBW setting, we first construct the discrete scan grids in delay and angle, and generate a clustered multipath channel realization according to (53)–(55). Using the resulting MPC parameters $\{\tau_l, \theta_{T,l}, \phi_{T,l}, \theta_{R,l}, \phi_{R,l}, \gamma_l\}_{l=1}^L$, we synthesize the angle-resolved wideband measurement by sampling the multi-dimensional channel response on the prescribed scan grid, consistent with the response model in (12)–(15).

Fig. 7 shows representative synthesized angular power spectra obtained from the angle-resolved measurement under different antenna HPBWs (with identical HPBWs in Co-El and Az at both Tx and Rx). For narrow beams (e.g., HPBW = 15°), the spectrum exhibits sharp angular selectivity and limited leakage to adjacent bins. As the HPBW increases (e.g., HPBW = 30° and 60°), the beam overlap and sidelobe leakage increase, causing the observed spectrum to broaden and the per-bin power to be redistributed over a wider angular region even for the same underlying channel realization. In the isotropic case, the spectrum approaches a flat response reflecting isotropic reception on the scan grid.

These examples visualize why simple power summation over scan angles is biased without compensating for the overlap effect, motivating the correction in (56).

To evaluate the synthesized-isotropic received power, we form the multi-dimensional power vector by taking the element-wise squared magnitude of the synthesized MDCIR samples. Here, for each HPBW setting, we generated 1,000 independent channel realizations. For each realization, we performed 100 trials by applying i.i.d. random phases to all MPCs to enforce the US assumption, and the reported results are averaged over trials. The synthesized omnidirectional channel power is then estimated by summing over the scan grid and compensating for beam overlap using the beam-accumulation factor as

$$\hat{P}_c = \frac{1}{\zeta} \sum_{k=1}^{N_{tot}} [\mathbf{P}]_k, \quad (56)$$

where ζ is computed on the same discrete scan grid using the adopted Gaussian beam model. We evaluate two compensation variants: (i) the on-grid (bin-centered) accumulation factor ζ , and (ii) the within-bin averaged factor $\bar{\zeta}$ that accounts for off-grid directions (scalloping). For each HPBW value, the estimation error is evaluated in dB as

$$\varepsilon_{dB} \triangleq 10 \log_{10} \left(\frac{\mathbb{E}[\hat{P}_c]}{\mathbb{E}[P_c]} \right), \quad (57)$$

where P_c in (2), and averaged over Monte-Carlo trials.

Fig. 8 summarizes the Monte-Carlo results of ε_{dB} for several directional scanning configurations. The reference curve computed from the true MPC powers remains close to 0 dB, validating the Monte-Carlo averaging under the uncorrelated scattering assumption. The correction using the on-grid accumulation factor ζ mitigates the dominant overlap bias but can leave a residual offset when MPC directions are off-grid (scalloping) and/or when the Co-El scan grid suffers from pole-related discretization artifacts. Using the averaged factor $\bar{\zeta}$ further reduces this residual bias, improving robustness with respect to HPBW and scan coarseness, particularly in wide-beam cases and in Co-El scanning.

B. Measurement Based Evaluation

To validate the proposed synthesized-isotropic power compensation with measured data, we compare the omnidirectional PL synthesized from D-D horn-to-horn (H2H) angle-scanning measurements with a reference measurement that uses an omnidirectional antenna at the Tx (O2H). In the H2H configuration, both the Tx and Rx employ high-gain horn antennas and perform full-Az scanning, whereas the O2H reference replaces the Tx horn with an omnidirectional antenna and scans only the Rx horn, thereby reducing angular-combining ambiguity.

Measurements were conducted in a line-of-sight (LoS) corridor at 154 GHz [23], with the Tx–Rx separation swept from 6–21 m in 1 m steps. For the H2H scan, both ends used 26 dBi horns ($HPBW \approx 9^\circ$) shown in Fig. 4 and were rotated over 360° with a 9° angular sampling interval. For the O2H reference, the Tx was modeled as omnidirectional ($HPBW = 360^\circ$) and only the Rx horn was rotated over 360° with the same 9° step.

Based on (24), the PLs were computed as

$$PL_{H2H} = -10 \log_{10} \left(\frac{1}{\zeta_{\phi_T} \zeta_{\phi_R}} \sum_{\check{\tau}, \check{\phi}_T, \check{\phi}_R} P(\check{\tau}, \check{\phi}_T, \check{\phi}_R) \right), \quad (58)$$

$$PL_{O2H} = -10 \log_{10} \left(\frac{1}{\zeta_{\phi_R}} \sum_{\check{\tau}, \check{\phi}_R} P(\check{\tau}, \check{\phi}_R) \right), \quad (59)$$

with the summation taken over the delay and available scan domains, where $P(\cdot)$ denotes an element of the multi-dimensional power grid obtained by reshaping the stacked power vector \mathbf{P} in (17). The within-bin average correction factors were employed.

Fig. 9 compares the synthesized and reference PL results. Fig. 9(a) shows the PL as a function of Tx–Rx separation, where the H2H result closely follows the O2H trend across the measured distance range. This indicates that the proposed method effectively compensates for the non-orthogonality and overlap of the scanned beams, enabling consistent omni-equivalent power recovery from discretely sampled D-D measurements. Fig. 9(b) plots the CDF of the PL difference, defined as $PL_{H2H} - PL_{O2H}$, which directly quantifies the residual bias and variability of the synthesis procedure. The concentration of the error distribution around 0 dB confirms that the proposed compensation substantially mitigates systematic overestimation (from beam overlap) and underestimation

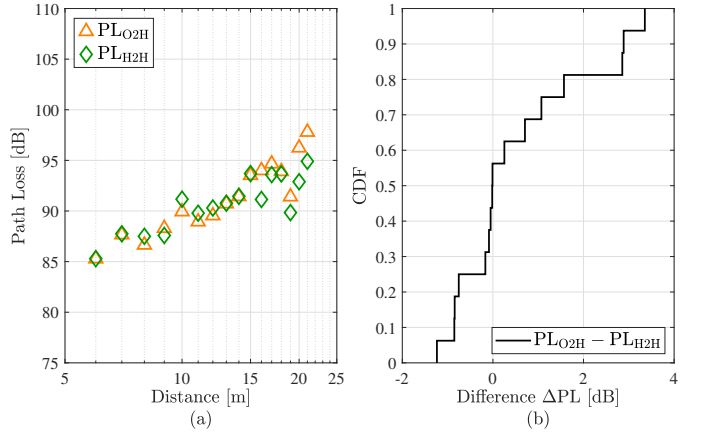


Fig. 9. Comparison of omnidirectional PL synthesized from D-D angle scanning (H2H) and the reference omnidirectional measurement at the transmitter (O2H): (a) PL versus Tx–Rx separation and (b) CDF of the PL estimation difference.

(from scalloping), leaving only measurement-to-measurement fluctuations due to finite angular resolution, sidelobe leakage, and environmental variability.

VI. CONCLUSION

This paper investigated antenna-independent channel parameter extraction (e.g., received power and PL) from angle-resolved wideband channel measurements, focusing on angular-domain bias in practical angle-scanning. While delay-domain power integration is largely straightforward after back-to-back calibration, naive angular summation is biased due to non-orthogonal, overlapping scan beams, and is further affected by scalloping for off-grid angles under a finite ASI. To address this, we formulated the synthesized-isotropic narrowband received power in a matrix form and introduced a beam-accumulation correction factor computed via discrete scan-grid summation of the squared antenna pattern, together with an offset-averaged variant to reduce scalloping sensitivity without explicit off-grid angle estimation. Simulations verified reduced overlap-induced bias and improved robustness versus HPBW and ASI, and 154 GHz LoS corridor measurements confirmed improved agreement between synthesized omnidirectional PL from H2H D-D scans and the O2H reference.

REFERENCES

- [1] T. S. Rappaport, *Wireless Communications: Principles and Practice*, 2nd ed. Upper Saddle River, NJ, USA: Prentice Hall, 2002.
- [2] V. Erceg, L. J. Greenstein, S. Y. Tjandra, S. R. Parkoff, A. Gupta, B. Kulic, A. A. Julius, and R. Bianchi, “An Empirically Based Path Loss Model for Wireless Channels in Suburban Environments,” *IEEE J. Sel. Area Commun.*, vol. 17, no. 7, pp. 1205–1211, Jul. 1999.
- [3] ITU-R, “The concept of transmission loss for radio links,” Recommendation ITU-R P.341-7, Aug. 2019.
- [4] ITU-R, “Multipath propagation and parameterization of its characteristics,” Recommendation ITU-R P.1407-8, Sept. 2021.
- [5] M. Steinbauer, A. F. Molisch, and E. Bonek, “The double-directional radio channel,” *IEEE Antennas Propag. Mag.*, vol. 43, no. 4, pp. 51–63, Aug. 2001.
- [6] M. Kim, Y. Konishi, Y. Chang, and J. Takada, “Large Scale Parameters and Double-Directional Characterization of Indoor Wideband Radio Multipath Channels at 11 GHz,” *IEEE Trans. Antennas Propag.*, vol. 62, no. 1, Jan. 2014.

[7] T. Zwick, D. Hampicke, A. Richter, G. Sommerkorn, R. Thomä, W. Wiesbeck, "A Novel Antenna Concept for Double-Directional Channel Measurements," *IEEE Trans. Veh. Technol.*, vol. 53, no. 2, pp. 527–537, Mar. 2004.

[8] M. Kim, S. Tang, and K. Kumakura, "Fast Double-Directional Full Azimuth Sweep Channel Sounder Using Low-Cost COTS Beamforming RF Transceivers," *IEEE Access*, vol. 9, pp. 80288–80299, 2021.

[9] R. Thomä, M. Landmann, A. Richter, and U. Trautwein, "Multidimensional High-Resolution Channel Sounding," in Smart Antennas in Europe State of the Art, EURASIP Book Series on SP & C, K. T., Ed. Hindawi Publishing Corporation, 2005, vol. 3.

[10] T. Doecker, J. M. Eckhardt, C. E. Reinhardt, and T. Kürner, "Time-Domain Channel Sounder Calibration at Low Terahertz Band," *IEEE Open J. Antennas Propag.*, vol. 5, no. 6, pp. 1598–1611, 2024.

[11] B. Fleury, M. Tschudin, R. Heddergott, D. Dahlhaus, and K. Pedersen, "Channel Parameter Estimation in Mobile Radio Environments Using the SAGE Algorithm," *IEEE J. Sel. Area Commun.*, vol. 17, no. 3, pp. 434–450, 1999.

[12] A. Richter, "Estimation of Radio Channel Parameters: Models and Algorithms," Ph.D. dissertation, TU Ilmenau, 2005.

[13] M. Kim, T. Iwata, S. Sasaki, J. Takada, "Millimeter-Wave Radio Channel Characterization using Multi-Dimensional Sub-Grid CLEAN Algorithm," *IEICE Trans. Commun.*, vol. E103-B, no. 7, pp. 767–779, Feb. 2020.

[14] M. Kim, "Millimeter-wave propagation of 5G wireless access," in *Handbook of Radio and Optical Networks Convergence*, T. Kawanishi, Ed. Singapore: Springer, 2023, pp. 1–28.

[15] M. Käse, M. Landmann, and, R. Thomä, "Modelling and Synthesis of Dense Multipath Propagation Components in the Angular Domain," *the 3rd European Conference on Antennas and Propagation (EuCAP)*, pp. 2641–2645, Berlin, Germany, Mar. 2009.

[16] S. Sun, G. R. MacCartney Jr., M. K. Samimi, and T. S. Rappaport, "Synthesizing Omnidirectional Antenna Patterns, Received Power and Path Loss from Directional Antennas for 5G Millimeter-Wave Communications," in *Proc. IEEE GLOBECOM*, Dec. 2015.

[17] K. Haneda, S. L. H. Nguyen, J. Järveläinen, and J. Putkonen, "Estimating the omni-directional pathloss from directional channel sounding," in *Proc. 10th Eur. Conf. Antennas Propag. (EuCAP)*, 2016.

[18] D. Burghal, J. Gomez-Ponce, N. A. Abbasi and A. F. Molisch, "Estimation of Isotropic Pathloss From Directional Channel Measurements in Azimuth and Elevation," *IEEE Antennas Wirel. Propag. Lett.*, vol. 23, no. 7, pp. 2145–2149, Jul. 2024.

[19] H. Xu, J. Zhang, P. Tang, H. Xing, L. Tian and Q. Wang, "High-Resolution Multipath Angle Estimation Based on Power-Angle-Delay Profile for Directional Scanning Sounding," *IEEE Trans. Antennas Propag.* (early access).

[20] M. Li, F. Zhang, X. Zhang, Y. Lyu and W. Fan, "Omni-Directional Pathloss Measurement Based on Virtual Antenna Array With Directional Antennas," *IEEE Trans. Veh. Tech.*, vol. 72, no. 2, pp. 2576–2580, Feb. 2023.

[21] P. A. Bello, "Characterization of Randomly Time-variant Linear Channels," *IEEE Trans. Commun. Syst.*, vol. 56, no. 12, pp. 360–393, Dec. 1963.

[22] M. Kim, "Analysis of Multipath Component Parameter Estimation Accuracy in Directional Scanning Measurement," *IEEE Antennas Wireless Propag. Lett.*, vol. 17, no. 1, pp. 12–16, Jan. 2018.

[23] R. Takahashi, A. Ghosh, M. Mao, M. Kim, "Channel Modeling and Characterization of Access, D2D and Backhaul Links in a Corridor Environment at 300 GHz," *IEEE Trans. Antennas Propag.*, vol. 73, no. 4, pp. 1954–1968, Apr. 2025.

[24] M. Kim, M. Yomoda, M. Mao, N. Kuno, K. Kitao, and S. Suyama, "Quasi-Deterministic modeling of Sub-THz band access channels in street canyon environments," *arXiv preprint*, arXiv:2509.10752v2, 2025.

[25] A. Saleh and R. Valenzuela, "A Statistical Model for Indoor Multipath Propagation," *IEEE J. Sel. Areas Commun.*, vol. 5, no. 2, pp. 128–137, 1987.